A high-mobility electron gas at the $LaAlO_3/SrTiO_3$ heterointerface

A. Ohtomo[1,2,3] **& H. Y. Hwang**[1,3,4]

[1]*Bell Laboratories, Lucent Technologies, Murray Hill, New Jersey 07974, USA*
[2]*Institute for Materials Research, Tohoku University, Sendai, 980-8577, Japan*
[3]*Japan Science and Technology Agency, Kawaguchi, 332-0012, Japan*
[4]*Department of Advanced Materials Science, University of Tokyo, Kashiwa, Chiba, 277-8651, Japan*

Polarity discontinuities at the interfaces between different crystalline materials (heterointerfaces) can lead to nontrivial local atomic and electronic structure, owing to the presence of dangling bonds and incomplete atomic coordinations[1–3]. These discontinuities often arise in naturally layered oxide structures, such as the superconducting copper oxides and ferroelectric titanates, as well as in artificial thin film oxide heterostructures such as manganite tunnel junctions[4–6]. If polarity discontinuities can be atomically controlled, unusual charge states that are inaccessible in bulk materials could be realized. Here we have examined a model interface between two insulating perovskite oxides—$LaAlO_3$ and $SrTiO_3$—in which we control the termination layer at the interface on an atomic scale. In the simple ionic limit, this interface presents an extra half electron or hole per two-dimensional unit cell, depending on the structure of the interface. The hole-doped interface is found to be insulating, whereas the electron-doped interface is conducting, with extremely high carrier mobility exceeding 10,000 $cm^2 V^{-1} s^{-1}$. At low temperature, dramatic magnetoresistance oscillations periodic with the inverse magnetic field are observed, indicating quantum transport. These results present a broad opportunity to tailor low-dimensional charge states by atomically engineered oxide heteroepitaxy.

An early discussion of polarity or valence discontinuities arose in the consideration of the growth of GaAs on (001)-oriented Ge[1,2]. Both semiconductors have the same crystal structure and nearly exact lattice match, thus representing promising materials to combine direct and indirect bandgap semiconductor functions. Just at the interface, however, there are incomplete bonds at the termination of the group IV Ge layer and the commencement of III–V alternations of GaAs. There have been recent attempts to design interfaces on the atomic scale to compensate for these dangling bonds[7]. Layered oxide crystal structures can be viewed as an intimate sequence of valence discontinuities, often involving charge-transfer over a few atomic positions. The myriad of stacking sequences such as the perovskite-derived Ruddlesden–Popper phases, constructed as $A_{n+1}B_nO_{3n+1}$, for $0 \leq n \leq \infty$, involve accommodating this charge transfer while maintaining global charge neutrality[8,9]. Recently, lamellar contacts between members

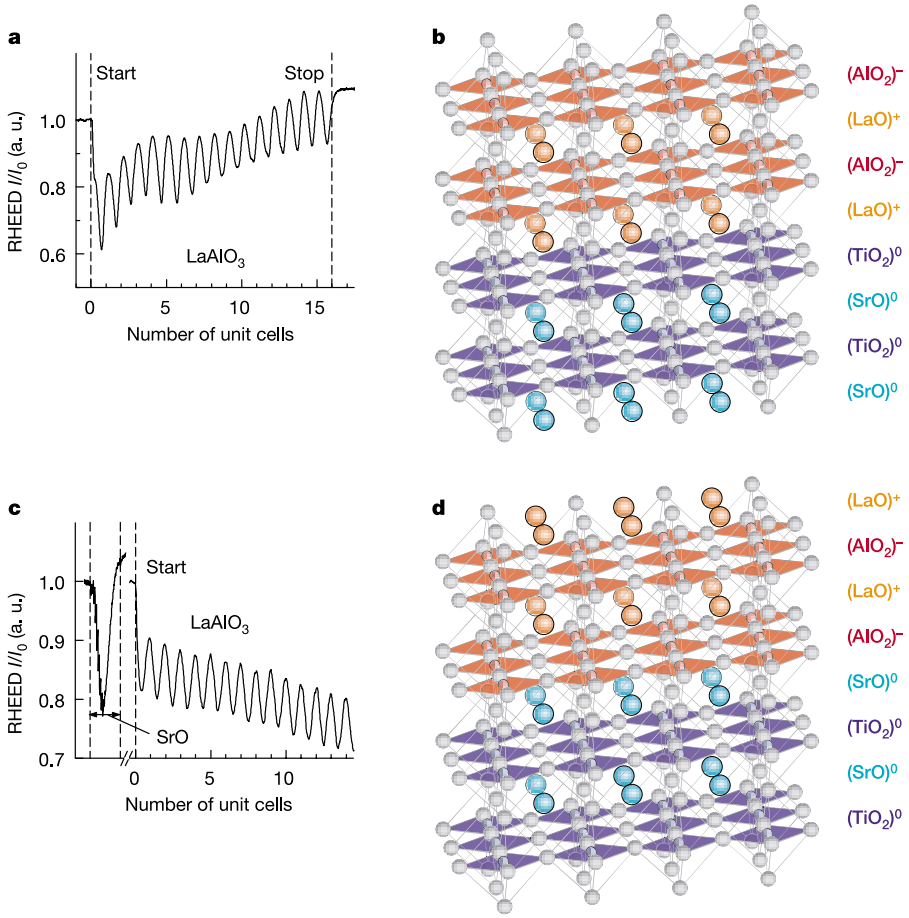

Figure 1 Growth and schematic models of the two possible interfaces between $LaAlO_3$ and $SrTiO_3$ in the (001) orientation. **a**, RHEED intensity oscillations of the specular reflected beam for the growth of $LaAlO_3$ directly on the TiO_2 terminated $SrTiO_3$ (001) surface. **b**, Schematic of the resulting $(LaO)^+/(TiO_2)^0$ interface, showing the composition of each layer and the ionic charge state of each layer. **c**, RHEED oscillations for the growth of $LaAlO_3$, after a monolayer of SrO was deposited on the TiO_2 surface. **d**, Schematic of the resulting $(AlO_2)^-/(SrO)^0$ interface.

of the ilmenite–haematite mineral series have been shown to induce interfacial magnetism via charge transfer[10].

Valence discontinuities naturally arise as a general concern in complex oxide heteroepitaxy as well. The electronic structure of an oxide heterointerface is important for its stability and function in many devices. In manganite tunnel junctions, for example, the magnetoresistance of the device is exponentially sensitive to the charge and spin state at the manganite–tunnel barrier interface[6]. The heterointerface between $LaAlO_3$ and $SrTiO_3$ is a simple, experimentally accessible realization of a valence discontinuity in perovskite oxides. Both are wide-bandgap insulators ($LaAlO_3 \approx 5.6$ eV, $SrTiO_3 \approx 3.2$ eV), and they are reasonably well lattice matched to one another (3.789 Å and 3.905 Å, respectively). The formal valence states can be assigned as La^{3+}, Al^{3+}, O^{2-}, Sr^{2+}, and Ti^{4+}; to first order, only Ti has accessible mixed-valence character, allowing for reduction towards Ti^{3+}. In the (001) direction, the perovskite structure ABO_3 can be considered as alternating stacks of AO and BO_2. $SrTiO_3$ is a sequence of charge-neutral sheets, whereas $LaAlO_3$ alternates between $\pm e$-charged sheets in the ionic limit, where e is the electron charge. The heterointerface of $LaAlO_3$ and $SrTiO_3$, therefore, presents an extra $\pm e/2$ per two-dimensional unit cell, again in the simple ionic limit (Fig. 1b and d).

The $LaAlO_3/SrTiO_3$ interfaces were grown in an ultrahigh vacuum chamber (Pascal) by pulsed laser deposition using a single-crystal $LaAlO_3$ target on (001) $SrTiO_3$ single-crystal substrates. $SrTiO_3$ substrates are well suited for this study, as techniques have been developed to etch TiO_2-terminated surfaces characterized by atomically flat terraces separated by unit cell steps[11]. The $(LaO)^+/(TiO_2)^0$ interface (Fig. 1b) was grown by direct deposition on this surface using a KrF excimer laser at a repetition rate of 2 Hz and a laser fluence at the target surface of $\sim 1\,J\,cm^{-2}$. The growth temperature was 800 °C as measured by a pyrometer (emissivity 0.8), with an oxygen partial pressure p_{O_2} ranging from 10^{-4}–10^{-6} torr. Typical unit cell reflection high-energy electron diffraction (RHEED) intensity oscillations are shown in Fig. 1a. The $(AlO_2)^-/(SrO)^0$ interface (Fig. 1d) was grown by first depositing a monolayer of SrO from a single-crystal target, then switching to $LaAlO_3$ *in situ*[12]. Typical RHEED oscillations for this case are shown in Fig. 1c. After growth of $LaAlO_3$, atomic force microscopy reveals that the original step and terrace structure of the substrate surface is preserved. This indicates that the intended interface is generally formed across the entire substrate.

We examined the conductivity of the interface, which required laser-annealed ohmic contacts through contact shadow masks to reach the buried interface (unpublished work). This contact method produced an array of microcracks penetrating the $LaAlO_3$ layer, as well as a tub of highly n-type $SrTiO_3$ formed by oxygen vacancies induced by the radiation. These contacts were formed around transport samples in typical six-probe Hall bar geometries. In all cases studied, the $(AlO_2)^-/(SrO)^0$ interface, expected to have a p-type interface, was insulating, although the possibility of Schottky barrier formation exists. The $(LaO)^+/(TiO_2)^0$ interface, however, indeed displayed n-type conductivity for a wide range of conditions. The temperature-dependent sheet resistance $R_{XX}(T)$ is given in Fig. 2a and b for 60-Å-thick and 260-Å-thick $LaAlO_3$ on $SrTiO_3$ for the $(LaO)^+/(TiO_2)^0$ interface at different p_{O_2} values during growth. The thicker $LaAlO_3$ film showed little p_{O_2} dependence, whereas the thinner film lost significant conductivity for higher p_{O_2} values. For the case of the films grown at 10^{-6} torr, a number of films are shown as a sample of the variability and reproducibility. The temperature dependence of the Hall coefficient R_H is given in Fig. 2c and d for the corresponding samples in Fig. 2a and b. There is little or no evidence for carrier freeze-out in most samples, consistent with the low activation barrier for dopants in $SrTiO_3$ (ref. 13). The resultant Hall mobility $\mu_H(T)$ is given in Fig. 2e and f, demonstrating the extremely high carrier mobility that can be obtained at the interface.

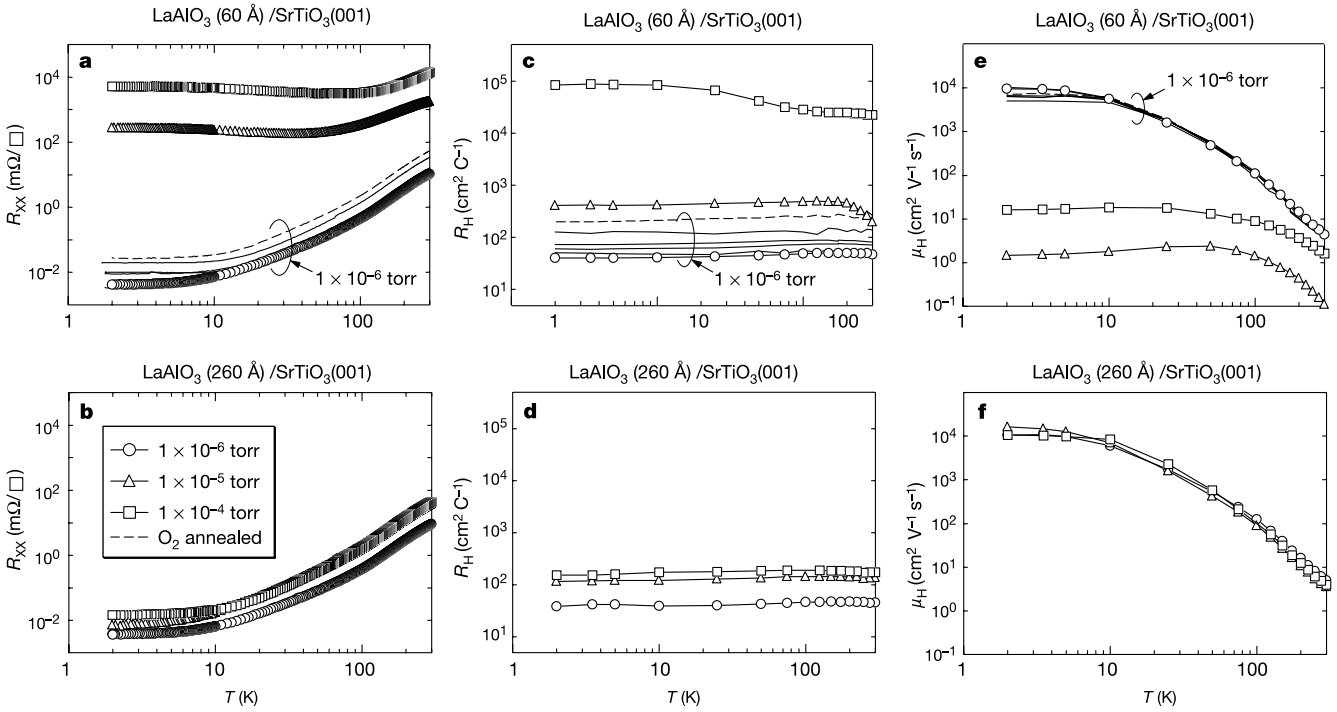

Figure 2 Transport properties of the $(LaO)^+/(TiO_2)^0$ interface for different oxygen partial pressures p_{O_2} during growth at 10^{-4}, 10^{-5}, and 10^{-6} torr, as well as for 10^{-6} torr growth followed by annealing in 1 atm of O_2 at 400 °C for 2 h. **a**, **c**, **e**, The temperature dependence of $R_{XX}(T)$, $R_H(T)$ and $\mu_H(T)$ for the interface between 60-Å-thick $LaAlO_3$ and $SrTiO_3$, respectively. **b**, **d**, **f**, The temperature dependence of $R_{XX}(T)$, $R_H(T)$ and $\mu_H(T)$ for the interface between 260-Å-thick $LaAlO_3$ and $SrTiO_3$, respectively.

One possible origin of the carriers is trapped oxygen vacancies at the surface of the substrate. To rule out this possibility, we confirmed that exposure of the substrate to the growth conditions (800 °C, 10^{-6} torr p_{O_2}, held for one hour, then quenched to room temperature) preserves an insulating surface. A related possibility is the formation of oxygen vacancies near the surface of $SrTiO_3$ by 'gettering' from incompletely oxidized $LaAlO_3$ in the growing film. This can be ruled out because the conductivity is removed when we insert a single monolayer of SrO before the $LaAlO_3$ growth. If oxygen gettering is the dominant origin of the carriers, then n-type conductivity should be obtained for both interfaces, which was not observed. Finally, we note that when a fraction of a monolayer of SrO is inserted before $LaAlO_3$ growth, the carrier density decreases proportionally with increasing SrO coverage from 0 to 1 monolayer. Therefore we conclude that the dominant mechanism introducing carriers is the built-in polarity discontinuity of the interface.

The high carrier mobilities imply that quantum transport might be observed in moderate magnetic fields at low temperatures. Indeed, distinct magnetoresistance oscillations are observed at 2 K for the 60 Å films grown at 10^{-6} torr, with representative traces given in Fig. 3a for samples shown in Fig. 2. As can be seen, the spacing and magnitude of the response varies widely, sample-to-sample, and sometimes even within the same sample hysteretically in magnetic field H. We have found that these oscillations diminish in magnitude over the course of weeks, until they completely vanish, despite an unchanging $R_{XX}(T)$ and $\mu_H(T)$. In some cases, however, they are relatively stable, as shown in Fig. 3b for two temperatures. To check the dimensionality of the charge state, we performed rotation experiments in magnetic field, given in Fig. 3c. The magnetoresistance features clearly remain fixed during rotation, indicating three-dimensional behaviour.

These intriguing results introduce a number of unresolved questions. One of the simplest is given in Fig. 4, which shows the variation of $1/R_H e$ for the samples studied here. Interpreting this as the sheet carrier density n would imply unphysical densities (10^{17} cm^{-2} requires a unit cell carrier density of 1.7×10^{22} cm^{-3} over 600 Å of thickness). Although we cannot rule out a possible role for oxygen vacancies at the interface, this extreme level is unobtainable in our growth conditions, and thermodynamically unfeasible[14]. Annealing in 1 atm of O_2 at 400 °C for 2 h gives little change to the transport properties. One possible interpretation is that $1/R_H e$ diverges from the simple carrier density in this system, as seen at high doping levels in (La,Sr)TiO_3 (ref. 15). Extreme-high-temperature annealing does diminish the conductivity more dramatically, but we caution that this may be driven by La/Sr interdiffusion. The diffusion at the interface of just the neighbouring sites is sufficient to cancel the interface charge, and the resolution of this Coulomb energy cost may enhance diffusion significantly. At 10^{-4} torr for the 60-Å films, the value associated with $e/2$ per two-dimensional unit cell is approached (Fig. 4).

The absence of the magnetoresistance oscillations in the thicker films is also unaccounted for, despite comparable mobility. Explanations may include kinetic effects involving cation redistribution and oxygen stoichiometry at the interface, or band-bending effects from states on the $LaAlO_3$ surface[16]. In addition, the lineshape of the magnetoresistance oscillation is unusual. Generally, we find one

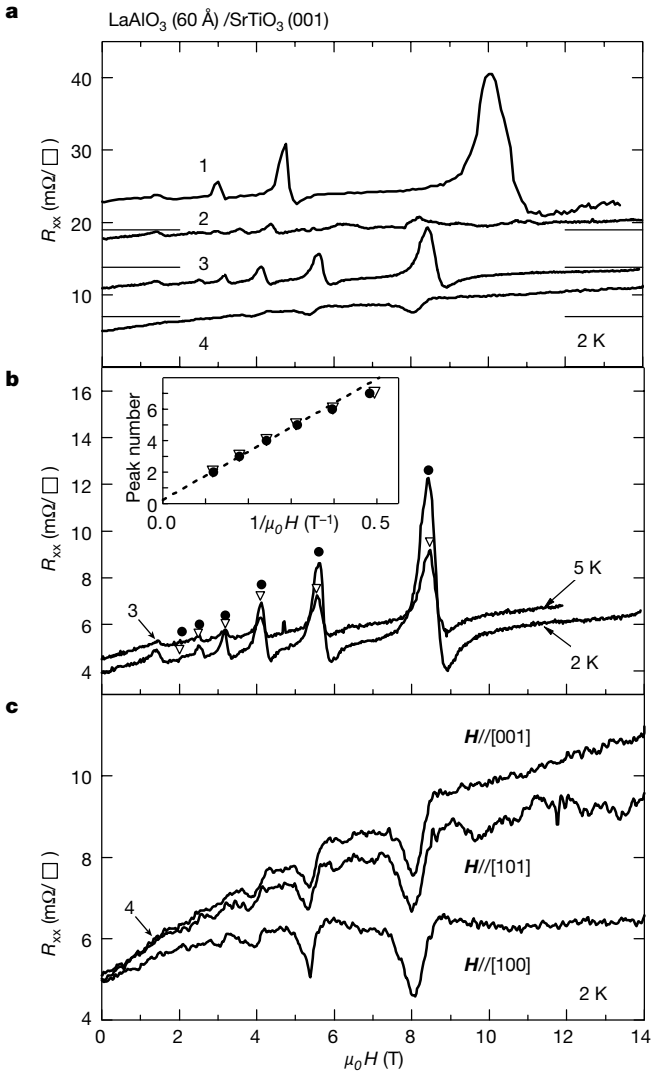

Figure 3 Low-temperature magnetoresistance of the $(LaO)^+/(TiO_2)^0$ interface between 60-Å-thick $LaAlO_3$ and $SrTiO_3$ grown at 10^{-6} torr p_{O_2}. **a**, Representative transverse magnetoresistance traces taken at 2 K. Curves 1–3 have been offset from the origin for clarity, with the positions of zero denoted by the corresponding horizontal lines. **b**, Magnetoresistance for sample number 3 in **a** at 2 K and 5 K. The peak positions are denoted by dots. Inset, the magnetoresistance peaks plotted versus the inverse magnetic field. **c**, Transverse magnetoresistance for sample number 4 in **a** for different field orientations: perpendicular to the interface (H//[001]), at 45° (H//[101]), and in the plane (H//[100]).

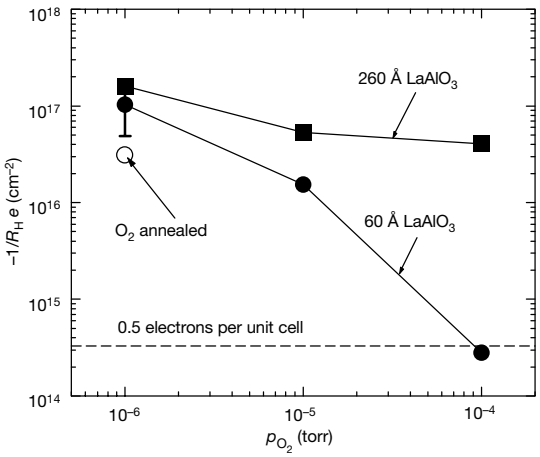

Figure 4 The dependence of $-1/R_H e$ at 2 K on the p_{O_2} during growth for the samples in this study. This quantity gives the carrier density $n = -1/R_H e$ for simple semiconductors. The sheet carrier density corresponding to 0.5 electrons per unit cell is denoted by the dashed line.

principal structure that is periodic in $1/H$. In comparable circumstances for bulk $SrTiO_3$, Shubnikov–de Haas oscillations associated with Fermi surface orbits give a sinusoidal variation[17]. Rather, we find a structure reminiscent of a Fano lineshape[18].

Despite these open questions, a number of issues can be deduced. Because there is little variation in the O2p-derived valence band across the perovskites, most of the band discontinuity must arise in the conduction band, placing the carrier in the $SrTiO_3$ conduction band. The periodicity in $1/H$ implies that this phenomenon can be associated with orbits in momentum space, rather than the H periodicity associated with real-space orbits[19]. These results are consistent with multiple sub-band occupancy arising from the high sheet carrier density, coupled with a very weak confining potential on the $SrTiO_3$ side due to the large (greater than 10,000), low-temperature static dielectric constant[20]. The varying behaviour in Fig. 3a is consistent with inhomogeneous current flow, arising from imperfectly uniform termination of the intended $(LaO)^+/(TiO_2)^0$ type[21]. Friction force microscopy indicates that occasional missed-termination sites can be found, particularly near the step edges. Transport geometries parallel and perpendicular to the step edges show no significant difference, indicating that scattering across step edges does not dominate transport. However, given the typical terrace width of 200 nm, many of these effects are necessarily averaged out in macroscopic transport samples. In this regard, although the magnetoresistance is measured to be macroscopically symmetric in H, mixing of the conductivity tensor may occur on a microscopic scale, especially considering the large Hall angles involved[22]. Nevertheless, it is a striking result that the periodicity in $1/H$ is unchanged by rotation in the field. This feature is associated with a constant cross-section of the Fermi surface in the standard interpretation, implying an electronic structure very different from that established for bulk $SrTiO_3$. We suggest that an unusual, non-bulk-like charge state is formed at this polar heterointerface. □

Received 10 October; accepted 19 December 2003; doi:10.1038/nature02308.

1. Baraff, G. A., Appelbaum, J. A. & Hamann, D. R. Self-consistent calculation of the electronic structure at an abrupt GaAs-Ge interface. *Phys. Rev. Lett.* **38,** 237–240 (1977).
2. Harrison, W. A., Kraut, E. A., Waldrop, J. R. & Grant, R. W. Polar heterojunction interfaces. *Phys. Rev. B* **18,** 4402–4410 (1978).
3. Kroemer, H. Polar-on-nonpolar epitaxy. *J. Cryst. Growth* **81,** 193–204 (1987).
4. Bednorz, J. G. & Mueller, K. A. Possible high-T_c superconductivity in the Ba-La-Cu-O system. *Z. Phys. B* **64,** 189–193 (1986).
5. Park, B. H. *et al.* Lanthanum-substituted bismuth titanate for use in non-volatile memories. *Nature* **401,** 682–684 (1999).
6. Tokura, Y. R. (ed.) *Colossal Magnetoresistive Oxides* Ch. 9, 10 (Gordon and Breach, New York, 2000).
7. Wang, T., Moll, N., Cho, K. & Joannopoulos, J. D. Deliberately designed materials for optoelectronics applications. *Phys. Rev. Lett.* **82,** 3304–3307 (1999).
8. Ruddlesden, S. N. & Popper, P. New compounds of the K_2NiF_4 type. *Acta Crystallogr.* **10,** 538–540 (1957).
9. Ruddlesden, S. N. & Popper, P. The compound $Sr_3Ti_2O_7$ and its structure. *Acta Crystallogr.* **11,** 54–55 (1958).
10. Robinson, P., Harrison, R. J., McEnroe, S. A. & Hargraves, R. B. Lamellar magnetism in the haematite–ilmenite series as an explanation for strong remanent magnetization. *Nature* **418,** 517–520 (2002).
11. Kawasaki, M. *et al.* Atomic control of the $SrTiO_3$ crystal-surface. *Science* **266,** 1540–1542 (1994).
12. Kim, D. W. *et al.* Roles of the first atomic layers in growth of $SrTiO_3$ films on $LaAlO_3$ substrates. *Appl. Phys. Lett.* **74,** 2176–2178 (1999).
13. Tufte, O. N. & Chapman, P. W. Electron mobility in semiconducting strontium titanate. *Phys. Rev.* **155,** 796–802 (1967).
14. Lide, D. R. (ed.) *CRC Handbook of Chemistry and Physics* , 77th edn (CRC Press, Boca Raton, 1996).
15. Tokura, Y. *et al.* Filling dependence of electronic properties on the verge of metal-Mott-insulator transitions in $Sr_{1-x}La_xTiO_3$. *Phys. Rev. Lett.* **70,** 2126–2129 (1993).
16. Francis, R. J., Moss, S. C. & Jacobson, A. J. X-ray truncation rod analysis of the reversible temperature-dependent [001] surface structure of $LaAlO_3$. *Phys. Rev. B* **64,** 235425 (2001).
17. Frederikse, H. P. R., Hosler, W. R. & Thurber, W. R. Shubnikov-de Haas effect in $SrTiO_3$. *Phys. Rev.* **158,** 775–778 (1967).
18. Fano, U. Effects of configuration interaction on intensities and phase shifts. *Phys. Rev.* **124,** 1866–1878 (1961).
19. Pippard, A. B. *Magnetoresistance in Metals* Ch. 6 (Cambridge Univ. Press, Cambridge, 1989).
20. Sakudo, T. & Unoki, H. Dielectric properties of $SrTiO_3$ at low temperatures. *Phys. Rev. Lett.* **26,** 851–853 (1971).
21. Nishimura, T. *et al.* Structure change of TiO_2-terminated $SrTiO_3(001)$ surfaces by annealing in O_2 atmosphere and ultrahigh vacuum. *Surf. Sci.* **421,** 273–278 (1999).
22. Herring, C. Effect of random inhomogeneities on electrical and galvanomagnetic measurements. *J. Appl. Phys.* **31,** 1939–1953 (1960).

Acknowledgements We thank D. Schlom, D. R. Hamann and T. Ohnishi for discussions. We acknowledge partial support from NEDO's International Joint Research Program. A.O. acknowledges partial support from the Asahi Glass Foundation and the Inamori Foundation.

Competing interests statement The authors declare that they have no competing financial interests.

Correspondence and requests for materials should be addressed to H.Y.H. (hyhwang@k.u-tokyo.ac.jp).

Atomic-scale imaging of carbon nanofibre growth

Stig Helveg[1], Carlos López-Cartes[1]*, Jens Sehested[1], Poul L. Hansen[1], Bjerne S. Clausen[1], Jens R. Rostrup-Nielsen[1], Frank Abild-Pedersen[2] & Jens K. Nørskov[2]

[1]*Haldor Topsøe A/S, Nymøllevej 55, and* [2]*Center for Atomic-scale Materials Physics, Department of Physics, Technical University of Denmark, DK-2800 Kgs. Lyngby, Denmark*

* Present address: Instituto de Ciencia de Materiales de Sevilla (CSIC-UNSE), Avda. Américo Vespucio s/n, Isla de la Cartuja, 41092 Sevilla, Spain

The synthesis of carbon nanotubes with predefined structure and functionality plays a central role in the field of nanotechnology[1,2], whereas the inhibition of carbon growth is needed to prevent a breakdown of industrial catalysts for hydrogen and synthesis gas production[3]. The growth of carbon nanotubes and nanofibres has therefore been widely studied[4–10]. Recent advances in *in situ* techniques now open up the possibility of studying gas–solid interactions at the atomic level[11–12]. Here we present time-resolved, high-resolution *in situ* transmission electron microscope observations of the formation of carbon nanofibres from methane decomposition over supported nickel nanocrystals. Carbon nanofibres are observed to develop through a reaction-induced reshaping of the nickel nanocrystals. Specifically, the nucleation and growth of graphene layers are found to be assisted by a dynamic formation and restructuring of mono-atomic step edges at the nickel surface. Density-functional theory calculations indicate that the observations are consistent with a growth mechanism involving surface diffusion of carbon and nickel atoms. The finding that metallic step edges act as spatio-temporal dynamic growth sites may be important for understanding other types of catalytic reactions and nanomaterial syntheses.

Here we formed carbon nanofibres by catalytic decomposition of methane over a catalyst consisting of Ni nanoclusters supported on $MgAl_2O_4$. This type of catalyst is widely used industrially in the steam reforming process[3]. The experiments are performed in an *in situ* transmission electron microscope (TEM)[13]. Nickel nanocrystals in the metallic state are formed by reduction of the NiO precursor at 500 °C in about 1 mbar H_2 for roughly 1 h in the TEM. The images show that the Ni nanocrystals have a faceted equilibrium shape (Fig. 1a). Methane is then added to the H_2 atmosphere to obtain a 1:1 mixture at a total pressure of about 2 mbar. TEM images show that graphitic nanofibres form with a Ni nanocluster located at the end and that the alignment of the graphene sheets into multi-layered carbon nanofibre structures couples to a reshaping of the Ni nanocluster. The present study considers Ni nanoclusters with diameters in the range of about 5 to 20 nm. Under these growth conditions, the smaller Ni nanoclusters tend to obtain a highly

ERRATUM

doi:10.1038/nature04774

Significant primordial star formation at redshifts $z \approx 3$–4

Raul Jimenez & Zoltan Haiman

Nature 440, 501–504 (2006)

In this Letter, the received and accepted dates were incorrect. They should read: 'Received 6 September 2005; accepted 4 January 2006.'

CORRIGENDUM

doi:10.1038/nature04726

Genome sequencing in microfabricated high-density picolitre reactors

Marcel Margulies, Michael Egholm, William E. Altman, Said Attiya, Joel S. Bader, Lisa A. Bemben, Jan Berka, Michael S. Braverman, Yi-Ju Chen, Zhoutao Chen, Scott B. Dewell, Alex de Winter, James Drake, Lei Du, Joseph M. Fierro, Robin Forte, Xavier V. Gomes, Brian C. Godwin, Wen He, Scott Helgesen, Chun Heen Ho, Stephen K. Hutchison, Gerard P. Irzyk, Szilveszter C. Jando, Maria L. I. Alenquer, Thomas P. Jarvie, Kshama B. Jirage, Jong-Bum Kim, James R. Knight, Janna R. Lanza, John H. Leamon, William L. Lee, Steven M. Lefkowitz, Ming Lei, Jing Li, Kenton L. Lohman, Hong Lu, Vinod B. Makhijani, Keith E. McDade, Michael P. McKenna, Eugene W. Myers, Elizabeth Nickerson, John R. Nobile, Ramona Plant, Bernard P. Puc, Michael Reifler, Michael T. Ronan, George T. Roth, Gary J. Sarkis, Jan Fredrik Simons, John W. Simpson, Maithreyan Srinivasan, Karrie R. Tartaro, Alexander Tomasz, Kari A. Vogt, Greg A. Volkmer, Shally H. Wang, Yong Wang, Michael P. Weiner, David A. Willoughby, Pengguang Yu, Richard F. Begley & Jonathan M. Rothberg

Nature 437, 376–380 (2005)

In this paper, the second name of Chun Heen Ho was misspelled as He. In the earlier Corrigendum (*Nature* **439,** 502; 2006) the surnames of Stephen K. Hutchison and Brian C. Godwin were misspelled as Hutchinson and Goodwin. In addition, in the Supplementary Information of the original paper, there were errors in the sequences of the DNA capture and enrichment primers, and in the formulation of emulsion oil. The Supplementary Information was updated on 4 May 2006.

CORRIGENDUM

doi:10.1038/nature04772

A phosphatase complex that dephosphorylates γH2AX regulates DNA damage checkpoint recovery

Michael-Christopher Keogh, Jung-Ae Kim, Michael Downey, Jeffrey Fillingham, Dipanjan Chowdhury, Jacob C. Harrison, Megumi Onishi, Nira Datta, Sarah Galicia, Andrew Emili, Judy Lieberman, Xuetong Shen, Stephen Buratowski, James E. Haber, Daniel Durocher, Jack F. Greenblatt & Nevan J. Krogan

Nature 439, 497–501 (2006)

Figure 3a of this Letter contains an inadvertently duplicated panel set: those referring to '*pph3*Δ (YJK26)' are identical to '*PPH3* (YJK17)'. The corrected panels are shown here. Note that the quantification shown in Fig. 3b refers to the correct panels. Our results and conclusions are unaffected by this oversight.

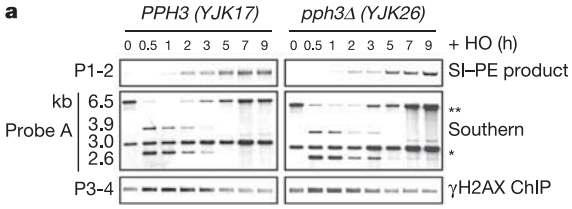

CORRIGENDUM

doi:10.1038/nature04773

A high-mobility electron gas at the $LaAlO_3/SrTiO_3$ heterointerface

A. Ohtomo & H. Y. Hwang

Nature 427, 423–426 (2004)

In Fig. 2a and b of this Letter, the *y* axis should be labelled in units of ohms per square, not milli-ohms per square. This error does not occur elsewhere in the paper, and does not change any of our results or conclusions.